



Covalently and non-covalently immobilized clusters onto nanocarbons as catalysts precursors for cinnamaldehyde selective hydrogenation



Charles Vriamont^{1,2}, Tommy Haynes¹, Emily McCague-Murphy, Florence Pennetreau, Olivier Riant, Sophie Hermans*

IMCN Institute, Université catholique de Louvain, Place L. Pasteur 1, 1348 Louvain-la-Neuve, Belgium

ARTICLE INFO

Article history:

Received 9 March 2015

Revised 18 May 2015

Accepted 1 June 2015

Keywords:

Clusters
Cinnamaldehyde
Nanoparticles
Bimetallic catalysts
Hydrogenation
Graphene
Carbon nanotubes
Non-covalent immobilization
Grafting

ABSTRACT

Ru-based nanoparticles were deposited on carbon nanotubes and graphene via an organometallic approach involving mixed-metal clusters modified with appropriate ligands. These ligands allowed either covalent or non-covalent π - π interactions with the carbonaceous surfaces. The immobilized clusters were then coalesced at different temperatures to give carbon-supported nanoparticles of different sizes. The obtained catalysts were tested in the selective hydrogenation of cinnamaldehyde. It was found that the nature of the metal(s), support nature, incorporation method and activation temperature all had a profound influence on activity and selectivity. Interestingly, the selectivity could be shifted from cinnamyl alcohol (COL) to hydrocinnamaldehyde (HCAL) by changing the reaction solvent. The best catalysts gave a very high selectivity in cinnamyl alcohol, which is not the more thermodynamically favored product, and could be reused several times without loss of activity or selectivity.

© 2015 Elsevier Inc. All rights reserved.

1. Introduction

Supported catalysts to be competitive should simultaneously fulfill the following criteria: a high activity and selectivity coupled to stability and ease of recovery over time [1]. The chemoselective hydrogenation of α,β -unsaturated aldehydes has been often selected to evaluate the above-mentioned criteria [1–5]. These compounds present two hydrogenable sites which means that two competitive reaction pathways can be followed: the selective transformation of the aldehyde into the corresponding unsaturated alcohol or the thermodynamically more favoured reduction of the olefin bond. These reactions pathways determine the chemoselectivity of the transformation and can be moreover complicated by side reactions occurring either on the metal active phase or on the support [3]. The Meerwein–Ponndorf–Verley reaction applied to these aldehydes in homogeneous catalysis allows to selectively obtain the unsaturated alcohol with a high conversion but a large amount of waste: This methodology is therefore prescribed for

costly chemicals [2,6,7]. The development of heterogeneous catalysts on various supports, environmentally friendlier and able to selectively hydrogenate both functions separately was thus considered as a valuable option by many authors [1–3,5,8–17].

Since the transformation in the two hydrogenated products, that is hydrocinnamaldehyde and cinnamyl alcohol, is of chemical interest, cinnamaldehyde was chosen as benchmark substrate. The abbreviations used, namely cinnamaldehyde (CAL), hydrocinnamaldehyde (HCAL), cinnamyl alcohol (COL) and hydrocinnamyl alcohol (HCOL), as well as the structure of the molecules, are shown in Fig. 1. COL is generally described as the most challenging product to obtain and is moreover the most valuable: It is a critical intermediate in the production of chemicals such as flavors, pharmaceuticals and perfumes [1,18]. Nevertheless C=C double bond hydrogenation to obtain HCAL as a product was recently reported as intermediate in the synthesis of medicines for the treatment of HIV, which makes it also a challenging product [19].

The chemoselectivity toward both products is affected by a considerable number of parameters such as particles metal(s) nature and type of faces exposed, steric and electronic effects, catalyst preparation, activation procedure, selected support or even reaction conditions [1,2,7,21]. A comprehensive review written by Gallezot et al. deals with this topic [2]. Among these parameters, the most explored is undoubtedly the metal nature. Studies

* Corresponding author. Fax: +32 10 47 2330.

E-mail address: sophie.hermans@uclouvain.be (S. Hermans).

¹ These authors contributed equally.

² Present address: Imperial College London, South Kensington Campus, London SW7 2AZ, UK.

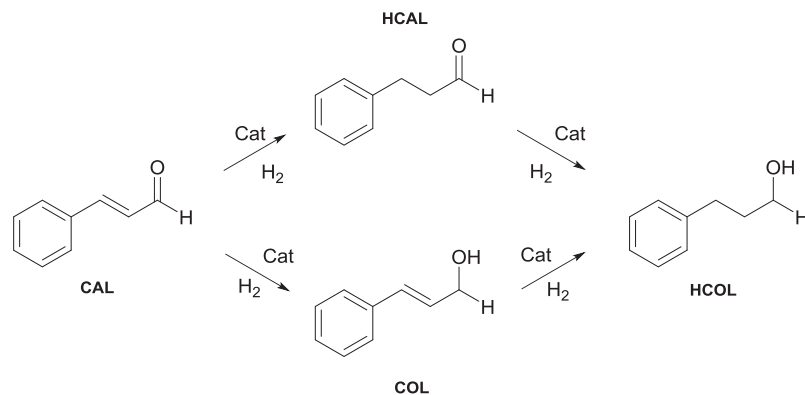


Fig. 1. The structure and conversion routes of α,β -cinnamaldehyde.

conducted on metals deposited on carbon supports revealed that Pt and Ru, because of their acceptable activity, selectivity and stability, feature among the best considered metals to obtain the desired unsaturated alcohol [21]. In addition, a combination of several metals can greatly improve the selectivity toward the desired product [12,18,20,22,23]: Pt–Ru bimetallic catalysts gave impressive activity and selectivity [1,24–27]. This activity/selectivity enhancement is a result of synergism effect [28] which can be explained mainly by electronic and geometric effects: The former is due to an alloy formation or intimate contacts between metals [29] while the latter comes from effects such as a modification of the metal dispersion [30,31] or a surface enrichment [32–34]. In general, both effects go hand in hand. Synthetic routes to obtain supported bimetallic nanoparticles are well documented and range from simple to more sophisticated methods such as ion exchange, impregnations methods, homogeneous deposition precipitation or even colloidal microwave process [22,35]. In almost all cases, these multi-metallic nanoparticles arise from separate monometallic precursors. The different metals are thus not necessarily in a close contact which is assumed to be of importance for catalysis [3]. The use of clusters [36] as nanoparticles precursors can *de facto* circumvent this problem. Relatively few studies deal with their use as single precursors for high performance nanocatalysts [37–42].

The catalyst support, whose main task consists in dispersing the metal on its surface, displays also a significant and sometimes critical role on both the activity and the selectivity in the targeted selective hydrogenation [3,4]. Oxides, such as silica and alumina, and carbon based supports including activated carbon, carbon nanofibers, carbon nanotubes (CNTs) and recently graphene

oxide/reduced graphene oxide (GO/rGO) are the most commonly used supports [1–3,5,8–17,43]. Among them, nanocarbons (CNTs, GO, rGO) have been selected for this work. It seems interesting to evaluate in terms of activity and selectivity the possible difference between these supports arising from metal dispersion and electronic effects. Indeed, graphene is a 2D system compared to the 1D CNTs [2]. Moreover, oxygenated functions, present in high amounts in GO (and rGO on a smaller scale), could also be of importance for the selectivity [44,45].

The present work reports an unconventional methodology to covalently and non-covalently anchor Ru-based mono- and Ru–Pt, Ru–Au and Ru–Pt–Au multi-metallic precursors onto nanocarbons. The undertaken route is depicted in Fig. 2, which shows schematically the successive steps envisaged. To this end, multi-walled carbon nanotubes (MWNTs) and graphene were selected as supports. Two pathways were attempted to obtain the target materials: a non-covalent and a covalent methodology. When the covalent pathway was undertaken, a pre-functionalization step is required (I): Acyl chloride functions were formed on GO or MWNTs on oxygenated functions located at defects- and end-sites. A recently reported radical approach involving xanthate chemistry applied to MWNTs was also selected to pre-functionalize nanocarbons [46]. In the next step, mono- and multi-metallic clusters were selected as single source metal precursors and immobilized onto nanocarbons by a covalent or a non-covalent strategy (II). In the latter case, a polar solvent and polyaromatics, that is pyrenes moieties, are required to perform this non-covalent immobilization involving π – π stacking [47]. All these catalysts, once thermally activated at different temperatures

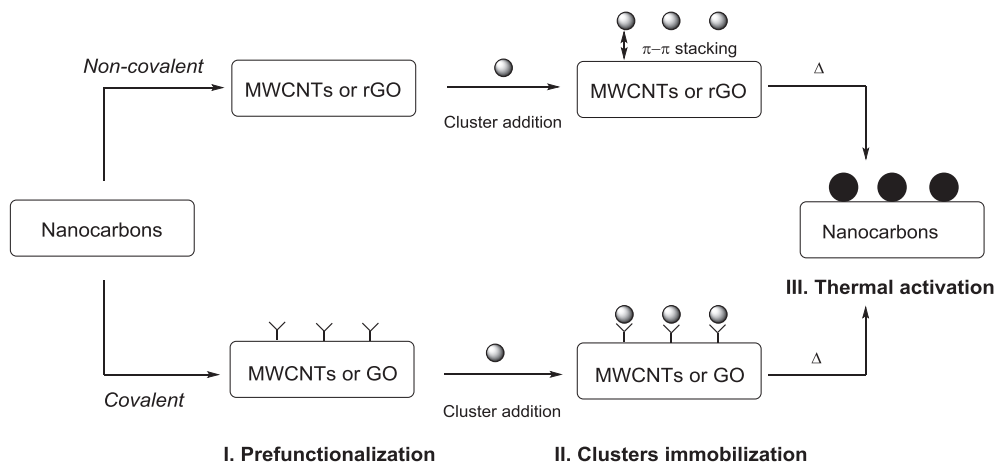


Fig. 2. General methodology to obtain mono- or multi-metallic nanoparticles arising from a single source metal precursor.

(III), were tested in the selective hydrogenation of cinnamaldehyde to assess and compare their activity and selectivity in order to find the best route to obtain selectively either COL or HCAL products. The recycling was finally tested for the best catalysts found.

If ruthenium and platinum have been selected as metals for their well-known properties toward the selective hydrogenation of α,β -unsaturated aldehydes, researches conducted on gold in these hydrogenation reactions have been appearing only in the last few years [48–51]. Au possesses remarkable activity in the targeted reaction. Nevertheless, the high selectivity obtained toward the desired COL product was found to be correlated with the use of oxide supports. Gold on nanocarbons as catalysts have been far less studied and an opposite trend, namely a high selectivity toward HCAL product, was reported in the only paper dealing with gold deposited on nanotubes [52].

2. Experimental section

2.1. Generalities and instrumental

MWNTs were obtained from Nanocyl (Belgium) (Thin MWNTs, 95+% C purity). Graphene Oxide (GO) and Reduced Graphene Oxide (rGO) were purchased from Nanolnnova technologies (Spain). Unless otherwise stated, all the manipulations were carried out under an atmosphere of Ar using standard Schlenk techniques and with anhydrous solvents. Hexane was distilled from sodium benzophenone, dichloromethane was distilled from CaH₂ and anhydrous acetone was used as received (Fisher Chemicals).

Samples before and after the thermal activation were analyzed by X-ray photoelectron spectroscopy (XPS) which was carried out at room temperature with a SSI-X-probe (SSX 100/206)

photoelectron spectrometer from Surface Science Instruments (USA) equipped with a monochromatized microfocus Al X-ray source. Samples were stuck onto small sample holders with double-face adhesive tape and then placed on an insulating home-made ceramic carousel (Macor®, Switzerland). Charge effects were avoided by placing a nickel grid above the samples and using a flood gun set at 8 eV. The energy scale was calibrated with reference to the Au_{4f7/2} peak at 84 eV and the binding energies were calculated with respect to the C–(C,H) component of the C1s peak fixed at 284.8 eV. Data treatment was performed with the CasaXPS program (Casa Software Ltd., UK). The peaks were decomposed into a sum of Gaussian/Lorentzian (85/15) after subtraction of a Shirley type baseline.

The elemental analyses (C, H, N, O, F, S, P, Ru, Pt, Au) were realized by MEDAC Ltd., UK. Nuclear magnetic resonance (NMR) spectra were recorded on BRUKER spectrometers (121 MHz for ³¹P). Mass spectra (MS) were recorded on a Q-Exactive orbitrap from ThermoFisher. Samples were ionized by ESI (capillary temperature: 250 °C, vaporizer temperature: 250 °C, sheath gas flow rate: 20). The clusters and their corresponding adducts were analyzed by infrared spectroscopy on a Bruker Equinox 55 spectrometer with a solution cell from Perkin Elmer. The powder catalysts were analyzed by transmission electron microscopy (TEM) with a LEO922 energy filter transmission electron microscope. The powder samples were suspended in hexane under ultrasonic treatment, then a drop of the supernatant was deposited on a holey carbon film supported on a copper grid, which was dried overnight under vacuum at room temperature before analysis. Gas Chromatography (GC) was performed on a GC trace, Finnigan Mat equipped with an AS-3000 Autosampler (FID detector). The GC column is a Chirasil-Dex CB, 25 m × 25 mm × 0.25 μm (Agilent). Gas vector: Helium, flow: 1.2 ml/min, injector split/split less ratio 1/30. The

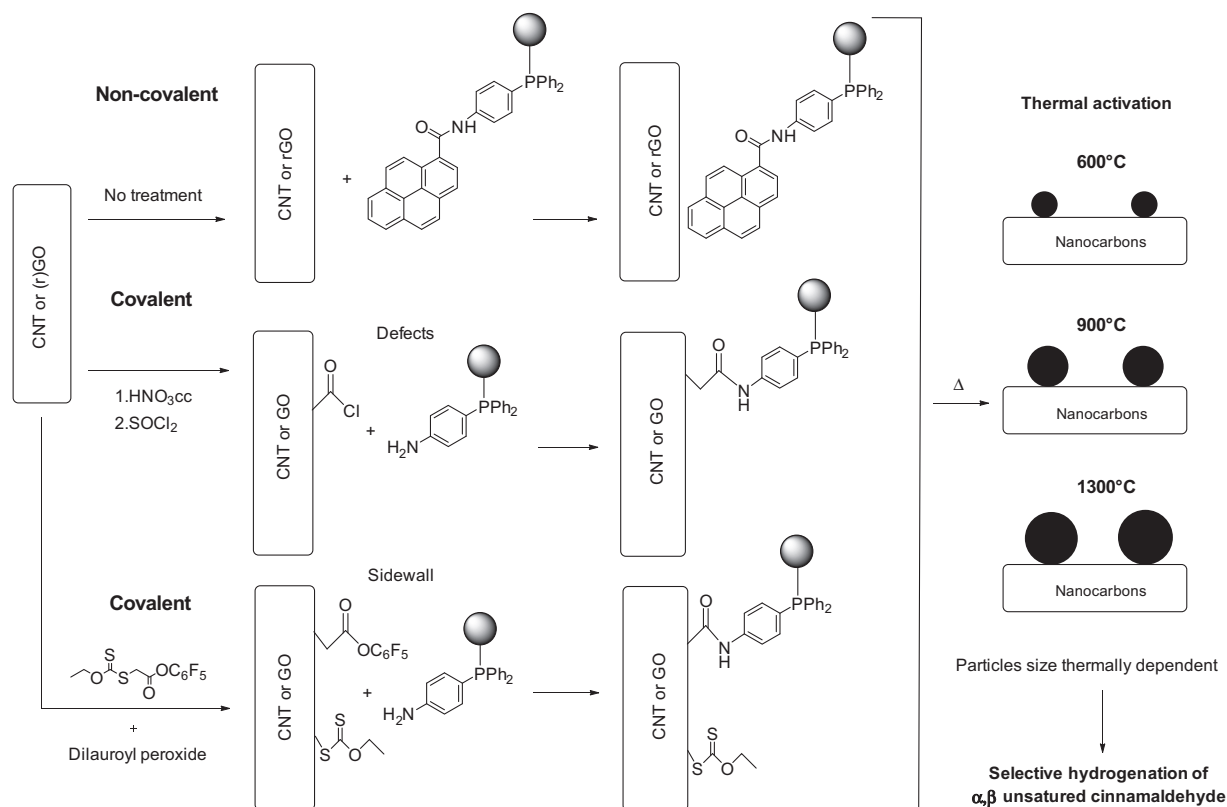


Fig. 3. Overview of the different pathways used to form multi-metallic nanoparticles on nanocarbons (gray spheres = cluster precursors; black spheres = metal nanoparticles).

internal standard used is dodecane and the temperature program is 120 °C (12') → 120 °C to 150 °C (5') → 150 °C (10').

The proposed methodology to synthesize mono- and multi-metallic nanoparticles supported on nanocarbons is unconventional: A detailed overview is presented in Fig. 3 and will serve as a guiding thread in the following sections. The preparation of the functionalized supports referenced **MWNT-Cl** and **GO-Cl** is described in SI, Section 3.2. The decoration of carbon nanotubes with activated esters using xanthate **13** is described in SI Section 3.3, to give **MWNTs-X**.

2.2. Clusters and bifunctional ligands syntheses

The two bifunctional ligands **1** and **2** were synthesized as reported previously [53]. The mono-, bi-, and tri-metallic clusters [Ru₆C(CO)₁₇] (**3**), [Ru₅PtC(CO)₁₆] (**4**), [Ru₆C(CO)₁₆(Au{PPh₃})₂] (**5**) and [Ru₅PtC(CO)₁₅(Au{PPh₃})₂] (**6**) were obtained according to literature procedures [54,59–61].

2.3. Ligands-clusters adducts (7–12) synthesis

The synthesis of adducts **7–12** was conducted using standard schlenk techniques. The clusters [Ru₆C(CO)₁₇] (**3**), [Ru₅PtC(CO)₁₆] (**4**), [Ru₆C(CO)₁₆(Au{PPh₃})₂] (**5**) or [Ru₅PtC(CO)₁₅(Au{PPh₃})₂] (**6**) (200 mg, 1 eq (1.871 · 10⁻⁴ mol (**3**); 1.7232 · 10⁻⁴ mol (**4**); 1.0075 · 10⁻⁴ mol (**5**); 9.7509 · 10⁻⁵ mol (**6**)) were dissolved in 25 ml of dichloromethane in a Schlenk round bottom flask. One equivalent of ligand **1** (for clusters (**3**) and (**4**)) or **2** (for clusters (**3–6**)) was added to the solution and then stirred for variable duration (5 min (**4**), overnight (**3–5**), 48 h (**6**)). The solvent was removed under reduced pressure. A volume of 20 mL of hexane was added and the solution was finally filtrated to recover a solid corresponding to the ligand-cluster coordination products **7–12**. Product **7**: yield: 98% (0.249 g); IR ν_{CO} (CH₂Cl₂) (cm⁻¹): 2056 (s), 2030 (s); ³¹P NMR (121 MHz, CDCl₃): δ = 47.71 (s); MS (ESI): *m/z* calcd for C₃₆H₂₀NO₁₆PRu₆ 1359.93 [M+1]⁺, found: 1359.84 [M+1]⁺; 1310.96 [M-NH₂-2CO+Na]⁺, 1286.00 [M-NH₂-3CO+Na]⁺, 1258.09 [M-NH₂-4CO+Na]⁺, 1228.11 [M-NH₂-5CO+Na]⁺, 1202.22 [M-NH₂-6CO+Na]⁺, 1171.09 [M-NH₂-7CO+Na]⁺, 1146.06 [M-NH₂-8CO+Na]⁺. Product **8**: yield: 97% (0.238 g); IR ν_{CO} (CH₂Cl₂) (cm⁻¹): 2057 (s), 2037 (s), 2003 (w, br), 1882 (w, br); ³¹P NMR (121 MHz, CDCl₃): δ = 29.44 (*t*, *J* = 3.197 MHz); MS (ESI): *m/z* calcd for C₃₅H₁₉NO₁₅PPtRu₅K 1466.50 [M+K]⁺, found: 1466.57 [M+K]⁺. Product **9**: yield: 97% (0.295 g); IR ν_{CO} (CH₂Cl₂) (cm⁻¹): 2056 (s), 2030 (s); ³¹P NMR (121 MHz, CDCl₃): δ = 47.27 (s); MS (ESI): *m/z* calcd for C₅₆H₃₂NO₁₇PRu₆Na 1651.56 [M+Na]⁺, found: 1651.93 [M+Na]⁺; 1622.92 [M-CO+Na]⁺, 1594.97 [M-2CO+Na]⁺, 1568.96 [M-3CO+Na]⁺. Product **10**: yield: 96% (0.284 g) IR ν_{CO} (CH₂Cl₂) (cm⁻¹): 2057 (s), 2037 (s), 2003 (w, br), 1882 (w, br); ³¹P NMR (121 MHz, CDCl₃): δ = 29.55 (*t*, *J* = 3.198 MHz); MS (ESI): *m/z* calcd for C₅₅H₃₂NO₁₆PPtRu₅Na 1716.63 [M+Na]⁺, found: 1715.99 [M+Na]⁺; 1662.01 [M-2CO+Na]⁺, 1286.00 [M-11CO+K]⁺, 1425.14. Product **11**: IR ν_{CO} (CH₂Cl₂) 2067 (vw), 2052 (s), 2007 (s, sh), 2001 (vs) (cm⁻¹); ³¹P NMR (121 MHz, CDCl₃): δ = 28.90, 42.12, 63.59, 64.02, 67.21; MS (ESI): *m/z* calcd for C₆₉H₄₇Au₂NNaO₁₂P₂Ru₆Na [M-5CO+Na]⁺ 2167.61 found: 2167.72. Product **12**: IR ν_{CO} (CH₂Cl₂) (cm⁻¹): 2068 (m), 2050 (m, sh), 2037 (s), 2014 (vs), 1967 (m); ³¹P NMR (121 MHz, CDCl₃): δ = 28.73, 29.39, 29.61, 30.76, 35.45, 39.51, 43.01, 68.59, 69.14, 69.70, 70.22, 71.46, 71.92, 73.32; MS (ESI): *m/z* calcd for C₈₆H₆₂Au₂NNaO₁₂P₃PtRu₅Na 2511.76 [M-C-3CO+Na]⁺, found: 2511.59 [M+Na-C-3CO]⁺; *m/z* calcd for C₁₀₇H₇₉Au₂N₂NaO₁₃-P₃PtRu₅ 2810.90 [M+Na-C-4CO-PPh₃+ligand **2**]⁺, found: 2810.73 [M+Na-C-4CO-PPh₃+ligand **2**]⁺.

2.4. Covalent immobilization of adducts **7** and **8** onto MWNT-Cl and G-Cl to obtain supported catalysts **C7**, **C8**, **GC7** and **GC8**

In a typical experiment, 200 mg of MWNT-Cl or G-Cl are introduced in a 100 mL Schlenk flask and submitted to ultrasound (Ultrasonic Cleaner, VWR) in dichloromethane (15 mL) for 1 h. The cluster **7** (200 mg, 0.147 mmol) or **8** (200 mg, 0.140 mmol) in dichloromethane (15 mL) was added and the suspension was stirred at room temperature for 2 h. The resulting mixtures were filtered out (on PVDF 0.22 μm pore size membrane) and washed twice with dichloromethane (2 × 20 mL) to separate the reactions products **7** and **8** from the supported adducts. These were vacuum dried to obtain **C7** and **C8** on MWNT-Cl and **GC7** and **GC8** on G-Cl corresponding to the immobilization of respectively **7** and **8** on the two different supports.

2.5. Covalent immobilization of adducts **7** and **8** onto MWNT-X to obtain supported catalysts **X7–X8**

In a typical experiment, 100 mg of MWNT-X was introduced in a Schlenk round bottom flask and submitted to ultrasound for 1 h (Ultrasonic Cleaner, VWR) in dichloromethane (15 mL). The cluster **7** (100 mg, 0.074 mmol) or **8** (100 mg, 0.070 mmol) in dichloromethane (15 mL) was added and the suspension was stirred at room temperature for 8 h. The resulting mixture was then filtered out over a PVDF (0.22 μm pore size) membrane and washed twice with dichloromethane (2 × 20 mL) to separate the reactions products **7** and **8** from the supported adducts. The resulting material was dried under vacuum overnight to get the supported adducts **X7** (from **7**) and **X8** (from **8**).

2.6. Non-covalent immobilization of adducts **9–12** to obtain supported catalysts **P9**, **PG9**, **P10**, **PO10**, **P11**, **P12**

In a typical experiment, 200 mg of pristine MWNTs (Nanocyl) or rGO (NanoInnova Technologies) was introduced in a 100 mL Schlenk flask and submitted to sonication in an ultrasonic bath (Ultrasonic Cleaner, VWR) in acetone (15 mL) for 1 h. The clusters **9** (200 mg, 0.1228 mmol), **10** (200 mg, 0.1165 mmol), **11** (200 mg, 0.0875 mmol) or **12** (200 mg, 0.0774 mmol), dissolved in acetone (5 mL) were added to the suspension and stirred at room temperature for 1 h. The resulting powders were submitted to centrifugation (6500 rpm, 10 min) and washed three times with acetone (6500 rpm, 10 min) to separate the non-immobilized clusters **9**, **10**, **11** and **12** from the supported adducts. Finally, the powders were dried under vacuum. The following supported adducts **P9**, **P10**, **P11** and **P12** on MWNTs and **PG9**, **PG10** on rGO were obtained and corresponded to the immobilization of respectively **9**, **10**, **11** and **12** onto MWNTs and **9** and **10** on rGO.

2.7. Thermal activation

The supported adducts were all submitted to a thermal treatment in a tubular oven STF 16/450 from CARBOLITE. The samples were placed into porcelain combustion boats and heated during 1 h at the selected temperature (heating ramp and cooling ramp: 100 °C/h) under a stream of N₂/H₂ (95:5) at 600 °C when supported on graphene GO-Cl and rGO and at 900 °C or 1300 °C when supported on MWNTs.

2.8. Hydrogenation of cinnamaldehyde: catalytic experiments

The catalytic experiments were realized in a 250 mL stainless steel PARR autoclave. The experimental conditions for hydrogenation depended on the solvent used and are summarized in Table S1 (SI). Two laboratory lines, N₂ and H₂ lines, were used with

regulatory high-pressure valves. In a 250 mL autoclave, cinnamaldehyde was introduced simultaneously with the desired solvent. The catalyst was then added and the autoclave was sealed. Afterward the system was purged 4 min with a stream of nitrogen, and then heated up to the desired temperature. Once the desired temperature had been reached, 50 bars of hydrogen were introduced and the mixture was stirred at 1500 rpm for 2 h. The hydrogen pressure is left to evolve naturally during the catalytic tests (slow decrease of pressure as H₂ is consumed). Hydrogen was subsequently slowly removed before cooling down the system to room temperature. The system was finally purged for 4 min with a stream of nitrogen. The solution was filtered out over a PVDF (0.22 μm pore size) membrane and the catalyst was washed with 50 mL solvent. The resulting solution was analyzed by GC.

3. Results and discussion

3.1. Clusters and bifunctional ligands

The selected bifunctional ligands **1** and **2** (Fig. 4) were synthesized on a multi-gram scale from the starting material 1-bromobenzonitrile, and were obtained following the synthetic route outlined in Fig. 4 [53]. Two functions of paramount importance were incorporated within **1** and **2**: a triphenylphosphine group since transition metals clusters are known to exchange readily their CO ligands to phosphine [54] and an amine (1) or pyrene (2) group to respectively interact covalently or non-covalently with nanocarbons. Pyrenes moieties were selected because it currently represents the only viable route to bring together nanotubes and polyaromatic moieties through π–π stacking [55–58].

Four clusters were selected as mixed-metal molecular precursors to obtain nanoparticles arising from a single source. The four clusters were obtained according to literature procedures [54,59–61]. These are depicted in Fig. 5 and are constituted of one, two or even three different metals: [Ru₆C(CO)₁₇] (**3**), [Ru₅PtC(CO)₁₆] (**4**), [Ru₆C(CO)₁₆(Au{PPh₃})₂] (**5**) and [Ru₅PtC(CO)₁₅(Au{PPh₃})₂] (**6**).

(6). The addition of platinum (**4**) or gold (**5**) or both metals (**6**) to the reference cluster **3** was realized to compare and follow the implication of these metals on the selectivity in the targeted selective hydrogenation.

3.2. Clusters-bifunctional ligand adducts syntheses

Adducts **7–12** were obtained according to the synthetic procedures given in Table 1 and proceeded through a quantitative exchange of ligands. This involves the phosphine of the ligand **1** or **2** and one of the constitutive carbonyl ligands of the clusters **3–4**. Two routes are possible when clusters **5** and **6** are involved: a phosphine-CO or phosphine-phosphine exchange. Adducts **7** and **9** were obtained instantaneously (5 min) while the obtention of **8**, **10–12** took more time (from overnight to 48 h). All the reactions were followed by IR spectroscopy and the final products were characterized by IR, ³¹P NMR and MS-ESI (see SI for characterizations).

IR spectra were recorded in the CO stretching zone between 2200 and 1600 cm⁻¹ to check the ligand exchange between bifunctional ligand **1** or **2** and a carbonyl/phosphine group of clusters **3–6**. A comparison made before and after adducts syntheses is reported in Table 1. A shift toward lower wave numbers (cm⁻¹) occurred due to modification of the clusters electronic environment in the cases of adducts **7–10**. When gold based clusters **11** and **12** were selected, the IR values observed before and after adducts syntheses were close (Table 2) (see SI: Section 1.2 for IR spectra). This might indicate ligand exchange with phosphines initially present in the starting clusters. Other characterization techniques, namely ³¹P NMR and MS have been implemented to solve this issue.

³¹P NMR and Mass Spectrometry (ESI-MS) were therefore recorded for all these compounds to give a deeper understanding of adducts formations. ³¹P NMR of products **7–10** (SI Section 1.3) showed a total disappearance of free ligands, no presence of oxidized ligands and their quantitative conversion into the

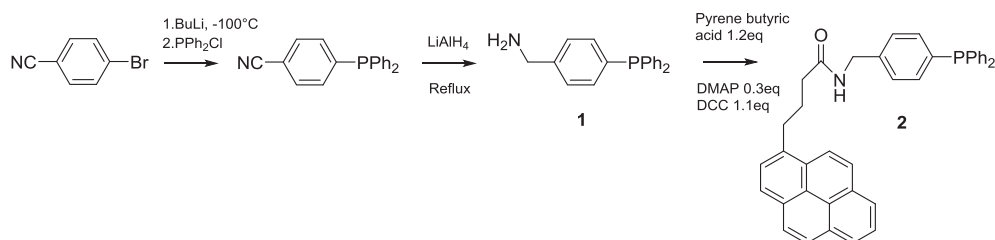


Fig. 4. Synthesis of the covalent **1** and non-covalent **2** bifunctional ligands.

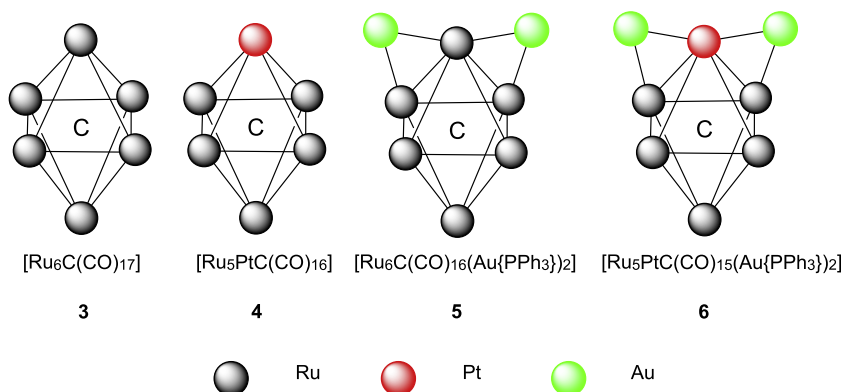


Fig. 5. The four selected mono-, bi- and tri-metallic clusters. CO ligands are omitted for clarity.

Table 1
Synthesis of adducts **7–12** by reaction between **1** or **2** as bifunctional ligand and **3–6** as cluster.

Cluster	Ligand	Adduct
3 = [Ru ₆ C(CO) ₁₇]	+ 1	= 7
4 = [Ru ₅ PtC(CO) ₁₅]	+ 1	= 8
3 = [Ru ₆ C(CO) ₁₇]	+ 2	= 9
4 = [Ru ₅ PtC(CO) ₁₅]	+ 2	= 10
5 = [Ru ₆ C(CO) ₁₆ (Au{PPh ₃ } ₂) ₂]	+ 2	= 11
6 = [Ru ₅ PtC(CO) ₁₅ (Au{PPh ₃ } ₂) ₂]	+ 2	= 12

Table 2
IR - ν_{CO} (cm⁻¹) before (clusters) and after coupling reaction (adducts) with bifunctional ligands.

	ν _{CO} (cm ⁻¹) clusters	ν _{CO} (cm ⁻¹) adducts
7	2066 (s), 2045 (s)	2056 (s), 2030 (s)
8	2065 (s), 2050 (vs), 2005 (w,br), 1869 (vw,br)	2057 (s), 2037 (s), 2003 (w,br), 1882 (w,br)
9	2066 (s), 2045 (s)	2056 (s), 2030 (s)
10	2065 (s), 2050 (vs), 2005 (w,br), 1869 (vw,br)	2057 (s), 2037 (s), 2003 (w,br), 1882 (w,br)
11	2067 (w), 2049 (s), 2017 (vs), 1965 (w), 1821 (m)	067 (vw), 2052 (s), 2007 (s,sh), 2001 (vs)
12	2068 (m), 2038 (s), 2015 (vs), 1968 (m), 1859 (m), 1834 (m)	2068 (m), 2050 (m,sh), 2037 (s), 2014 (vs), 1967 (m)

corresponding adducts. When bimetallic Ru–Pt clusters were selected, pseudo-triplet peaks were observed which corresponded to satellite peaks characteristic of the ¹⁹⁵Pt–³¹P coupling. This indicates the exact ligand exchange position, namely at the platinum site. When gold clusters **11** and **12** were selected, the ³¹P NMR analyses showed a total disappearance of both free ligand **2** and clusters **5** and **6**. The peak assignments were nonetheless not so straightforward due to the large number of ³¹P NMR peaks in both. The suggested mechanism involves an exchange of ligands between **2** and one of the initially present triphenylphosphine ligand within the clusters **5** and **6** to obtain **11** and **12**. Nevertheless a CO–ligand exchange is also possible and could explain the high number of observed peaks in these two last adducts.

Finally, mass spectrometry gave further evidence of the syntheses of adducts **7–12**. The observed signals (*m/z*) for compounds **7–10** gave not only the pseudo molecular ion (M+H⁺ for **7**, M+K⁺ for **8** and M+Na⁺ for **9** and **10**) but also some peaks from the gradual loss of CO ligands. If similar evidence was not observed for adducts **11** and **12**, that is no pseudo-molecular peaks, some fragments were obtained that confirmed the bond between bifunctional ligands and clusters **5** and **6**. Furthermore, the obtained fragments confirmed the proposed exchange between a triphenylphosphine ligand of **5** and **2** to get **11** (see SI Section 1.4). In addition, these analyses indicated the presence of two different possible adducts in the case of **12** (Phosphine–CO exchange and a double exchange: Phosphine–CO and Phosphine–phosphine within the same adduct). Their presence does not hamper the desired strategy and they can therefore be used to be immobilized on nanotubes and graphene.

Table 3
XPS analyses of the supports used for adducts immobilization.

XPS atomic ratio	Pristine MWNT	MWNT-ox	MWNT-Cl	MWNT-X	GO	GO-Cl	rGO
O/C	0.0125	0.0480	0.0472	0.0180	0.4863	0.3061	0.0900
Cl/C	/	/	0.0030	/	/	0.0194	/
F/C	/	/	/	0.0227	/	/	/
S/C	0.0014	/	/	0.0021	0.0082	/	/

Finally and in light of the obtained results, the required time to synthesize the different adducts can be explained and greatly depends on which metals are present in the clusters used. The coupling took place instantly on the Pt site when Pt–Ru bimetallic clusters were chosen which is probably due to a lower dissociative energy of the Pt–CO bond (578 kJ/mol) compared to Ru–CO bond (648 kJ/mol) [62–63]. It could therefore explain the time difference observed between adducts formations **7–8** and **9–10**. The synthesis of **11** is based on a phosphine–phosphine ligand exchange and cannot be compared with the four previous adducts. The required time to obtain adduct **12**, which contains platinum, does not follow the same model. The carbonyl group bonded to platinum in the tri-metallic cluster **6**, sterically hindered, is probably difficult to reach. Phosphine vs. CO (except for that of Pt) ligand exchange explains the required long vs. short time to complete these coupling reactions (see SI Section 2).

3.3. Adducts incorporations onto nanocarbons

Incorporations of adducts **7–12** were performed on nanocarbons (MWNTs and graphene) by non-covalent and covalent immobilizations, including sidewall and defect sites anchoring, as outlined in Fig. 2. If the non-covalent strategy does not require any pre-treatment, the opposite is true in the covalent cases.

3.3.1. Surface functionalization of nanocarbons

Given the amine pending groups present in adducts, we choose to incorporate acyl chloride and activated ester groups at the nanocarbon surface since these are known to readily react with amine groups to form robust amide bonds.

3.3.1.1. Surface modification (MWNTs and GO) to graft acyl chloride functions. An oxidative treatment to create acidic functions at the tubes surface was conducted on pristine MWNTs (95%+ purity), based on a previous study [64]. The selected treatment was chosen with the aim to oxidize the nanotubes without degrading them, namely the use of concentrated nitric acid under reflux for 2 h. This specific treatment is not requested when GO was used due to the initially existing oxygenated functions on this support (see Table 3). The acylation step, involving the use of SOCl₂, was applied in both cases and transformed carboxylic acid groups in acyl chlorides functions to furnish the functionalized supports referenced MWNT-Cl and GO-Cl [65] (see SI Section 3.2 for experimental procedures). All these samples were characterized by XPS before and after functionalization as shown in Table 3. As expected, the ratio O/C increased during the oxidative treatment of MWNTs. The acylation step was successfully performed with SOCl₂ as a reagent regardless of the support. The initial O/C ratio was considerably higher when GO was used (10 times higher than MWNTs-ox) and logically the chlorine atomic percentage obtained by XPS followed the same trend to afford a considerably higher number of acyl chlorides functions at the surface of graphene than nanotubes.

3.3.1.2. Surface modification of MWNTs through the radical xanthate chemistry. The xanthate **13** (see SI Section 3.3 for experimental) has already been proven reliable [46] and was thus selected to

decorate the tubes with activated esters (**MWNTs-X**). The XPS results obtained before and after functionalization are also reported in Table 3. The obtained F/C ratio was in agreement with previously reported values [46], and corresponded to a functionalization degree of 1 function every 22 carbons of the tubes given the average number of concentric tubes in a MWNT observed by TEM, that is approximately 10 (see SI Section 3.1).

3.3.2. Immobilization and characterization of the adducts 7 and 8 incorporated on nanocarbons by a covalent methodology to obtain C7 (MWNT-Cl + 7), GC7 (GO-Cl + 7), X7 (MWNT-X + 7), C8 (MWNT-Cl + 7), GC8 (GO-Cl + 8) and X8 (MWNT-X + 8)

The suggested mechanism for covalent immobilization involves an amine attack (from adducts 7 and 8) on acyl chloride or activated ester functions born by nanocarbons, followed by departure of chloride or fluorinated ester and formation of a covalent amide bond. The values obtained by XPS after covalent anchoring are given in Table 4. The presence of the expected metals, namely Ru and Pt, was confirmed by XPS. Moreover, when both metals are present, their Ru/Pt ratios were in agreement with the theoretical values (i.e. 5). The obtained Ru/P ratios were also generally close to the calculated values but nevertheless slightly lower. The F/C and Cl/C XPS ratios both decrease after functionalization (compare Tables 3 and 4), which indicates the expected covalent bond formation. The amount of metal (metal atomic percentage) covalently bonded to MWNTs was similar irrespective of the methodology of incorporation selected, as demonstrated by a simple Ru/C comparison between C7-X7 and C8-X8. The support used greatly influenced the quantity of grafted metal since the atomic percentage was two or three times higher when immobilization was performed onto graphene. This undoubtedly came as a result of an initially more functionalized surface (see Table 3).

3.3.3. Immobilization and characterization of adducts 9–12 incorporated on nanocarbons by a non-covalent methodology to obtain P9 (MWNTs + 9), PG9 (rGO + 9), P10 (MWNTs + 10), PG10 (rGO + 10), P11 (MWNTs + 11) and P12 (MWNTs + 12)

The selection of pyrene moieties in a polar solvent to immobilize these adducts onto nanocarbons was guided by some studies devoted to π - π stacking [47,48]. Metallic ratios (Pt/Ru and Au/Ru) determined by XPS after non-covalent immobilization of cluster/ligands adducts were close to the calculated values (see Table 4). The situation was also comparable regarding the Ru/P ratios and in both cases slightly lower than expected. Nevertheless, much lower Ru/P values were obtained when gold was present within the clusters (**P11–P12**), which cannot be fully explained. For all samples, the high increase of O/C values (to compare with pristine MWNTs and rGO in Table 3) clearly demonstrated the immobilization of clusters, with their substantial oxygen content within the CO ligands.

3.4. Thermal treatments

Adducts incorporated by covalent (**C7, X7, GC7, C8, X8** and **GC8**) or non-covalent (**P9, PG9, P10, PG10, P11** and **P12**) methodology onto nanocarbons were submitted to a thermal treatment. This treatment was required to remove both carbonyl ligands surrounding the clusters and the bifunctional ligand used to immobilize them on the supports in order to obtain naked metallic particles on the surface. Some related studies have demonstrated the benefit of such anchoring/thermoactivation techniques allowing a homogeneous dispersion of the resulting particles [65].

The selected activation temperature also influences not only the average particle sizes but also the number of remaining oxygen surface groups and both factors can influence the selective

Table 4
XPS analyses of the adducts incorporated onto nanocarbons.

Sample Code	C7	X7	GC7	C8	X8	GC8	P9	PG9	P10	PG10	P11	P12
O/C	0.092	0.069	0.184	0.079	0.055	0.0184	0.043	0.157	0.036	0.154	0.043	0.045
Cl/C	0.002	/	0.020	0.003	/	0.017	/	/	/	/	/	/
F/C	/	0.016	/	/	0.015	/	/	/	/	/	/	/
P/C	0.005	0.004	0.008	0.004	0.003	0.010	0.002	0.006	0.001	0.008	0.003	0.004
Ru/C	0.021	0.024	0.042	0.010	0.011	0.030	0.011	0.036	0.003	0.035	0.004	0.003
Ru/M ^{a,b}	/	/	/	3.9 ^a	4.1 ^a	3.7 ^a	/	/	3.6 ^a	4.1 ^a	2.4 ^b	1.6 ^b 3.1 ^a
Ru/P	4.3	6.3	5.2	2.5	3.8	3.0	4.6	5.6	3.3	4.3	1.3	0.8

^a Pt.

^b Au.

Table 5
The fifteen synthesized catalysts: sample code and preparation methodology.

Entry	Adduct	Support	Incorporation methodology	Code	Thermal Activation (°C)	Sample code
1	7 (Ru)	MWNT-Cl	Acyl chloride	C7	900	C7-900
					1300	C7-1300
2	7 (Ru)	MWNT-X	Xanthates	X7	900	X7-900
3	7 (Ru)	GO-Cl	Acyl chloride	GC7	600	GC7-600
4	8 (RuPt)	MWNT-Cl	Acyl chloride	C8	900	C8-900
5	8 (RuPt)	MWNT-X	Xanthates	X8	900	X8-900
6	8 (RuPt)	GO-Cl	Acyl chloride	GC8	600	GC8-600
7	9 (Ru)	MWNTs	Pyrene	P9	900	P9-900
					1300	P9-1300
8	9 (Ru)	rGO	Pyrene	PG9	600	PG9-600
9	10 (RuPt)	MWNTs	Pyrene	P10	900	P10-900
					1300	P10-1300
10	10 (RuPt)	rGO	Pyrene	PG10	600	PG10-600
11	11 (RuAu)	MWNTs	Pyrene	P11	600	P11-900
12	12 (RuPtAu)	MWNTs	Pyrene	P12	600	P12-900

hydrogenation of α , β -unsaturated aldehydes: The higher the temperature, the bigger the particles. But also, the higher the temperature, the least acidic and oxygen surface groups. If the increase in particle size was generally admitted to improve the selectivity toward the unsaturated alcohol, the oxygen surface groups effect is still a matter of debate [44,45].

To gain an overview of the temperature effect, three temperatures were selected: 600 °C, 900 °C and 1300 °C. The thermal activations were realized under reducing atmosphere with a mixture of nitrogen and hydrogen in a ratio 95/5. The two highest temperatures were applied to MWNTs while only the lowest value (i.e. 600 °C) was used for graphene: A higher temperature leads to a large weight loss. This can be explained by the very high amount of oxygen initially contained in graphene (see Table 3) leading to losses as CO and CO₂ at high temperature, but also of its exfoliated structure.

Fifteen catalysts were obtained by combining four clusters, three temperatures, three different types of immobilization procedures and two different nanocarbon supports. They are presented and codified for more clarity in Table 5. This includes the following information: metal(s) nature, support used, functionalization methodology and thermal activation temperature.

To get more information about the influence of the parameters tested on the catalysts obtained, TEM images were recorded and some of them are presented in Fig. 6. As expected, average particle sizes are indeed growing up when heating up. The methodology of incorporation also had an influence on the particle size

distribution. Indeed, π - π stacking and covalent anchoring methodology through acyl chlorides gave, for a given temperature and support, bigger particles than the sidewall radical functionalization methodology (see Fig. 6). Histograms (at the right of TEM images) were built by measuring in each case more than a hundred metal particles on several images of the selected sample using the AnalySIS Auto 5.0 software (Olympus Soft Imaging Solutions GmbH, Germany). A greater number of particles are indeed centered on 3–4 nm for π - π stacking and defects/end sites functionalization than for xanthate chemistry. These phenomena can be explained by the nature of the link established with nanocarbons. The π - π stacking is a weaker “link” than the covalent ones and logically led to bigger particles. The location of the covalent anchoring points, that is a uniform distribution for activated esters versus defect/end sites for acyl chlorides could play on the sintering: The latter are closer together, which can facilitate the coalescence and then increase the particle size. In addition, oxygenated functions are more easily cleaved. These considerations can explain the different particle sizes observed.

XPS analyses (Table 6) were also conducted after thermal treatment and revealed in most cases a decrease or disappearance of phosphorous peaks. A slight change in the Ru/Pt and a significant change in the Ru/Au ratios were observed after heating. These differences indicate some modifications in the clusters structures. These observations, at least in the case of RuPt nanoparticles, are in agreement with the selected technique (XPS) giving a surface, and not a bulk analysis. The coalesced nanoparticles might have

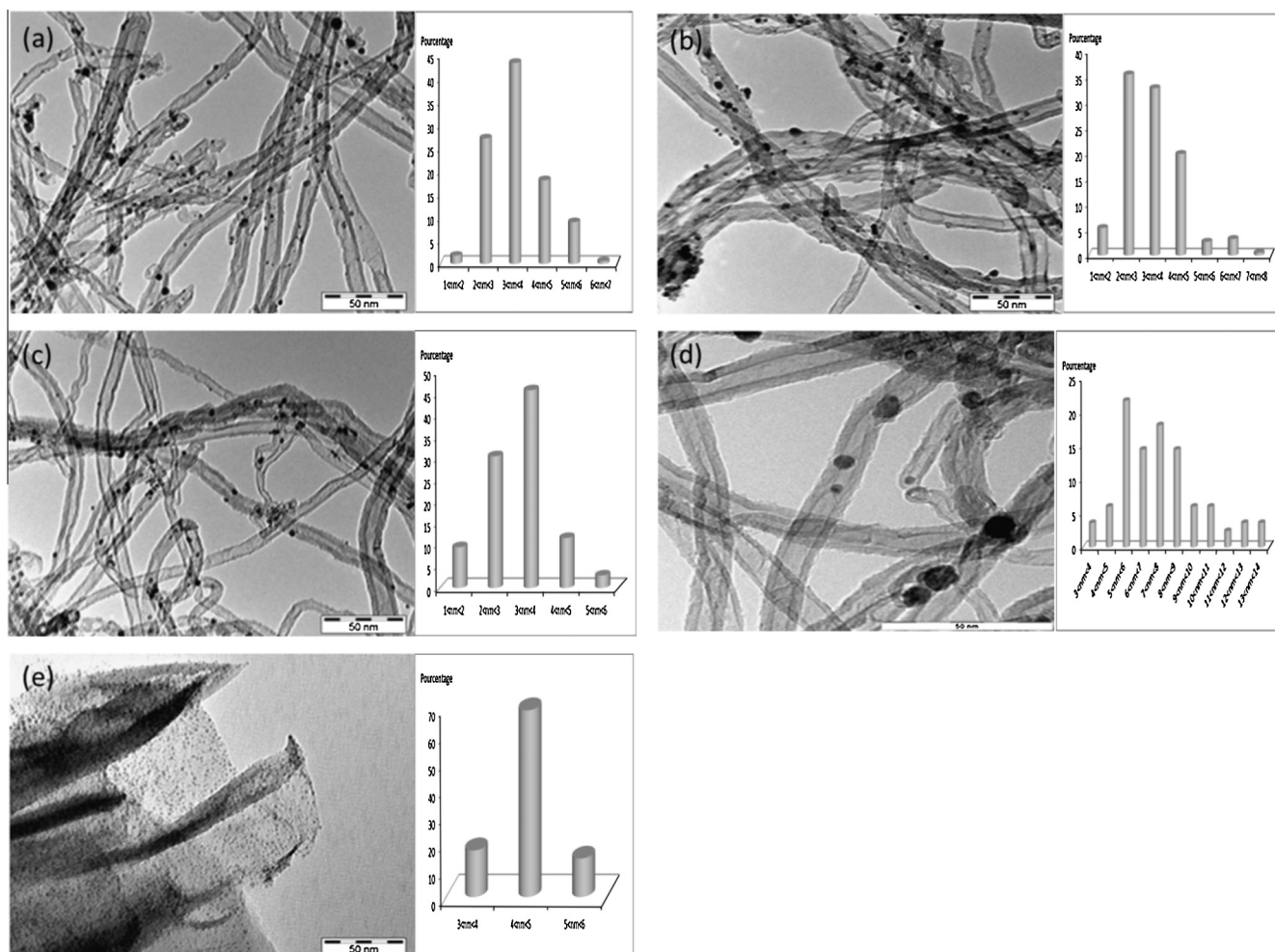


Fig. 6. TEM images of catalysts (a) C8-900, (b) X8-900, (c) P10-900, (d) P10-1300 and (e) GC8-600.

Table 6

XPS results obtained after thermal activation at different temperatures (600, 900 and 1300 °C).

Sample Code	C7-900	C7-1300	X7-900	GC7-600	C8-900	X8-900	GC8-600	P9-900	P9-1300	PG9-600	P10-900	P10-1300	PG10-600	P11-900	P12-900
O/C	0.011	0.501	0.025	0.089	0.048	0.019	0.168	0.011	0.028	0.100	0.015	0.026	0.083	0.018	0.017
P/C	0.002	0.002	/	0.002	0.056	/	0.016	0.002	0.002	0.014	/	/	0.006	0.002	0.002
Ru/C	0.021	0.024	0.042	0.010	0.011	0.030	0.011	0.036	0.003	0.035	0.004	0.003			
Ru/M ^{a,b}	/	/	/	/	6.9 ^a	4.1 ^a	3.9 ^a	/	/	/	4.7 ^b	2.7 ^a	5.6 ^a	7.5 ^b	6.5 ^b 3.3 ^a
Ru/P	4.4	5	/	2.9	1.5	/	2.0	2.7	5.3	3.6	/	/	4.1	0.9	0.6

^a Pt.^b Au.

surface enrichment in one or the other metal. Moreover, the biggest particles will only partially contribute to the XPS signal. Similar results were already obtained in a related study for Ru, Pt and Au based clusters [66].

ICP analyses (Ru) were also realized after thermal activation by the firm MEDAC LTD (UK) to determine metal loading of all the catalysts (see Tables in Sections 4.1 and 4.2 in Supporting Information). The obtained results sometimes differ from those obtained by XPS, as expected given the nano-supports and large particle sizes in some cases.

3.5. Selective hydrogenation of cinnamaldehyde

Activity and selectivity of ruthenium, ruthenium–platinum, ruthenium–gold and ruthenium–platinum–gold catalysts will be studied in this section. These greatly depend on a lot of parameters such as the metal incorporation methodology, the support used, the thermal activation temperature and the nanoparticles metallic nature. The effects of these factors will be discussed below. The experimental procedure for hydrogenation of cinnamaldehyde is given in SI, Section 4.

3.5.1. Activity of the catalysts

All the catalysts were tested in the selective hydrogenation of cinnamaldehyde and their activities were compared after 2 h at 120 °C under 50 bars of H₂ in 2-propanol/water (5/1 volume) as solvent (see SI Section 4, Table S1 and Experimental above). Note that the presence of water was needed to avoid alcohol by-products formation (acetal formation) [9]. The conversions ranged from 26% to 83% and are listed in Tables in Sections 4.1 and 4.2 in Supporting Information. For greater clarity, catalysts activities are split according to the support used: Table in Section 4.1 in SI includes the catalysts immobilized on graphene while nanotubes-based catalysts are presented in Table in Section 4.2 in SI. It is striking that the best conversions are always obtained with catalysts prepared by π - π stacking. TON and TOF (both calculated on the basis of the conversion to all products) values were

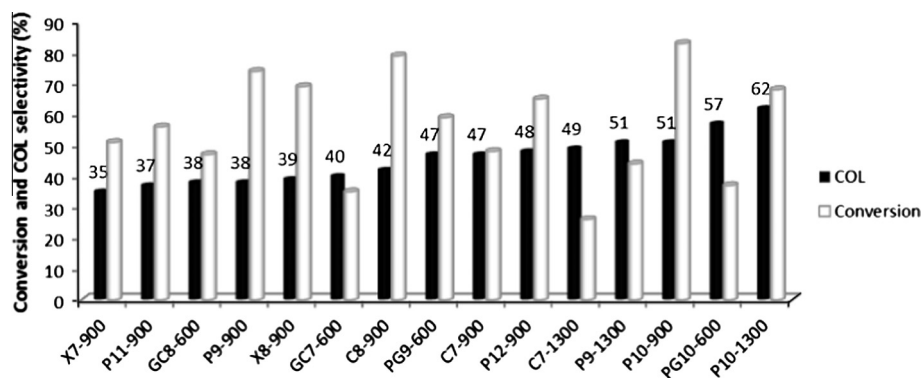
calculated from the ICP values for Ru content obtained by MEDAC (Tables in Sections 4.1 and 4.2 in Supporting Information). Some illustrative curves of conversion as function of time are also given in Supplementary Information.

3.5.2. Influence of various parameters on the selectivity

All the catalysts tested are plotted in Fig. 7 according to their increasing selectivity toward COL. Nature of the metal(s), incorporation methodology, nature of the support and temperatures of thermal activation have been analyzed separately in order to understand in more details the parameters influencing the reaction selectivity. Finally, some catalysts were also tested in a non-polar solvent to determine whether the solvent had any influence on the selectivity.

3.5.2.1. Nature of the metal. The selectivity was influenced to a considerable extent by the nature of the metal(s) used within the selected clusters. This effect is depicted in Fig. 8 where the only variable is the metal nature. Indeed all the presented catalysts were prepared by an identical pathway, namely non-covalently immobilization on pristine MWNTs and subsequent activation at 900 °C. The Ru–Pt partnership (**P10-900**) strongly improved the selectivity toward COL and gave, as expected, the best values [1,27,67] while the presence of gold within the bi-metallic Ru–Au nanoparticles (**P11-900**) shifted the selectivity toward HCAL (as previously observed [52]). Finally, the trimetallic catalyst **P12-900**, gave a better selectivity toward COL than **P9-900** and **P11-900** most probably due to the presence of platinum within the nanoparticles.

3.5.2.2. Effects of temperature, methodology of incorporation and nature of the support. It has been reported that the selectivity toward COL increases concomitantly with a growing particle size [2]. This particle size effect can be explained by a directing effect of the phenyl group [44]. The metal surface prevents access to the phenyl groups and thus repels the close C=C bond from the surface in the case of big nanoparticles, the C=O bonds being then

**Fig. 7.** Conversion and selectivity toward COL of the fifteen catalysts ($t = 2$ h).

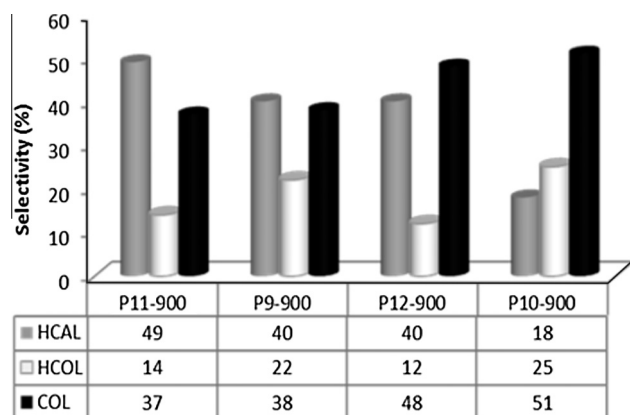


Fig. 8. Metal(s) effect in the selective hydrogenation of cinnamaldehyde.

able to approach the surface in priority in order to proceed to hydrogenation. These considerations do not apply in the case of small particles since no repelling between phenyl rings and particles can occur as depicted in Fig. 9.

The depicted effect was clearly observed here with all the catalysts. As shown by TEM, particle sizes are thermally dependent and the selectivity toward COL was strongly increased for catalysts activated at higher temperature, regardless of the selected incorporation methodology. A comparison between the catalysts **C7-900** and **C7-1300**, **P9-900** and **P9-1300** or **P10-900** and **P10-1300** clearly indicates an increase in the selectivity toward the desired COL product due to higher temperature of activation. The outstanding importance of the particle size effect can be proven when comparing bimetallic **P10-900** and monometallic **P9-1300** catalysts: The latter shows indeed exactly the same selectivity than the bimetallic one and was therefore able to compensate the lack of platinum. The particle size difference between catalysts thermoactivated at 900 and 1300 °C is important. Indeed, a comparison between **P10-900** and **P10-1300** shows a shift from particles broadly centered around 3–4 nm for the former to particle sizes between 5 and 9 nm for the latter (see Fig. 6).

As presented in Fig. 3, the methodology of immobilization had a real impact on catalytic properties. The non-covalent methodology was the best route to selectively hydrogenate the C=O bond since six of the eight best catalysts were prepared by this route. Defect sites functionalization and sidewall functionalization came after and in that order. A comparison between RuPt bimetallic catalysts onto nanotubes thermally activated at 900 °C **X8-900**, **C8-900** and **P10-900** clearly demonstrates this effect. It is worth noting that the routes involving radicals lead to catalysts more selective toward HCAL than COL, even if platinum was present (see Fig. 7).

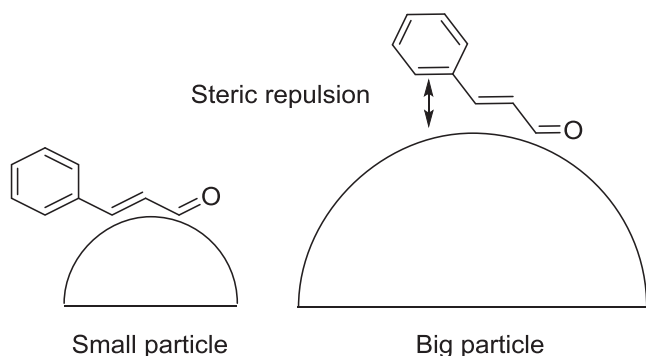


Fig. 9. Adsorption of cinnamaldehyde on a small metal particle (left) and a large particle (right) (adapted from Ref. [44]).

These results are related to the different cluster anchoring routes, which affect the particle size and consequently the selectivity. As depicted in Fig. 6, the particle size distribution was centered between 3 and 4 nm when a non-covalent anchoring was used while an average smaller particle size and broad distribution after the heating process were encountered in covalent cases. In addition, covalent routes might lead to remaining functions on the surfaces which also might be deleterious for the selectivity.

In order to selectively obtain the COL product, thermoactivations at 900 and 1300 °C were investigated when MWNTs were used. These temperatures were inadequate with graphene as support due to large weight loss. However, a comparison between **GC7-600** and **C7-900** or **P10-900** and **PG10-600** shows that the lower thermal activation is compensated by the use of graphene instead of MWNTs and revealed the positive effect of this support on the targeted product. Nevertheless, the possibility of heating MWNTs at temperatures higher than 600 °C is a decisive factor in view of the correlation between selectivity and large particles: This provides the best catalyst of this work (**P10-1300**).

The methodologies described here, nanocarbons functionalization following three different routes to anchor mono- or multi-metallic clusters are at an early stage. This first study in cinnamaldehyde hydrogenation was capable of rapidly increasing the selectivity toward the targeted product through a fine-tuning of the used conditions. On these bases, the best catalyst found gave good activity and selectivity, namely 68% conversion and 62% selectivity respectively. Compared to literature [1,27,45,67], there is still room for improvement compared to the best results reported so far, namely 95% [1,67] and 93% [27] selectivity toward COL using Ru–Pt catalysts. Nevertheless, in these two cases, the metal weight ratios are 1/1 (Pt/Ru), that is higher than in our case.

3.5.2.3. Solvent effect. It is generally considered that the solvent greatly affects the activity and moderately the selectivity of the catalyst in the selective hydrogenation of cinnamaldehyde [2]. The mix 2-propanol/water previously used was replaced by one of the best non-polar solvent to perform the selective hydrogenation of cinnamaldehyde: toluene [2]. The experimental conditions used are the following: 50 bars H₂, 110 °C and 1500 rpm. The results obtained in this case are depicted in Fig. 10. Compared with the previous results achieved when 2-propanol/water was chosen as a solvent, the activity was plummeted to barely reach 32% conversion after 2 h in the best case. Surprisingly the selectivity was completely modified to selectively obtain the HCAL product in all cases with selectivities between 71% and 85%. Even if a slight decrease in the selectivity toward COL was awaited, this reversal was not expected and shows the importance of solvent selection in the selective hydrogenation of cinnamaldehyde. Nevertheless, and because both HCAL and COL products are of synthetic

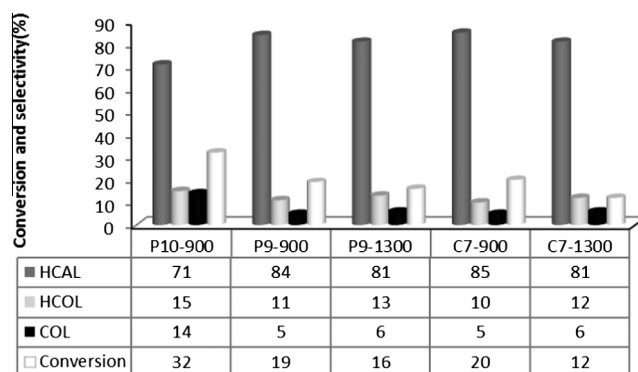


Fig. 10. Conversion and selectivity toward HCAL, HCOL and COL of some catalysts tested in toluene as solvent ($t = 2$ h).

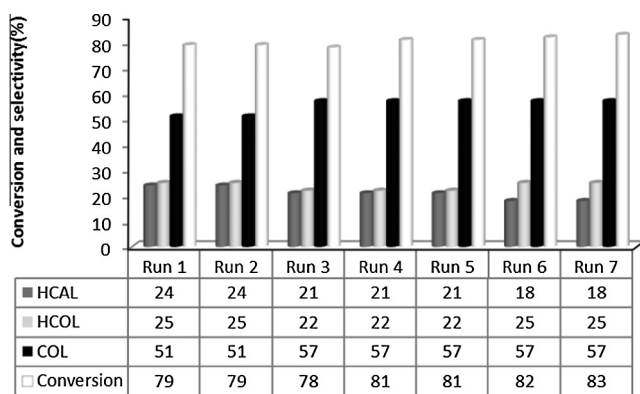


Fig. 11. Recycling of catalyst P10-900.

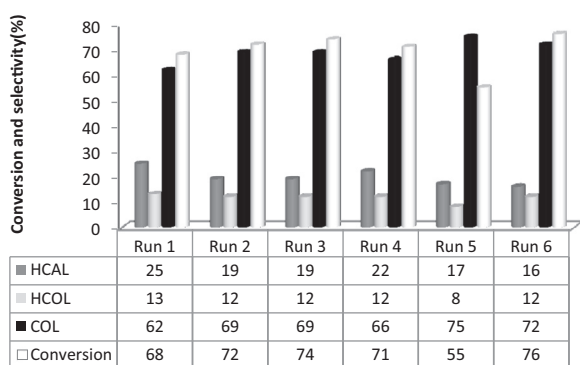


Fig. 12. Recycling of catalyst P10-1300.

importance, this solvent dependence is of real interest. Two of the best catalysts described in this study, namely **P10-900** and **P9-1300** can therefore selectively transform CAL into COL or HCAL by a simple solvent change.

3.5.3. Recycling

Catalyst reusability is of paramount importance. It was therefore attempted with two of the best catalysts found, that is **P10-900** and **P10-1300**. The results are given in Figs. 11 and 12. In the first case, we obtained a constant activity, around 80% conversion, coupled with a selectivity that remains constant. After the two first cycles, the selectivity even marginally increased to reach 57% selectivity toward COL. This slight increase was probably due to a small modification of the catalyst after the two first catalytic cycles to give it its final characteristics. The same tendency was observed with the catalyst **P10-1300** to reach, after the first run, a selectivity approaching 70% toward COL (with a peak at 75% selectivity) and a conversion of about 70% along the runs.

4. Conclusion

We have reported unusual methodologies to form mono- or multi-metallic nanoparticles onto nanocarbons (nanotubes and graphene) and these were used as catalysts in the selective hydrogenation of cinnamaldehyde. Four clusters, that is $[\text{Ru}_6\text{C}(\text{CO})_{17}]$ (**3**), $[\text{Ru}_5\text{PtC}(\text{CO})_{16}]$ (**4**), $[\text{Ru}_6\text{C}(\text{CO})_{16}(\text{Au}(\text{PPh}_3)_2)]$ (**5**) and $[\text{Ru}_5\text{PtC}(\text{CO})_{15}(\text{Au}(\text{PPh}_3)_2)]$ (**6**) were selected as nanoparticles precursors with the aim to retain their metallic stoichiometries and intimate contacts in the final catalysts. These cluster complexes were reacted with bifunctional ligands to quantitatively form adducts (**7–12**) able to interact by a covalent or a non-covalent

pathway with nanocarbons. A pre-functionalization step was required in the covalent case: The well-known oxidative treatment and its subsequent acylation step to provide acyl chloride at the support surface (**MWNTs-Cl** and **G-Cl**) and the xanthate chemistry applied to MWNTs to obtain activated esters at their surface (**MWNTs-X**) were applied. Covalent anchoring and non-covalent anchoring were carried out and the solids were subsequently activated at different temperatures (600 °C for graphene, 900 and 1300 °C for MWNTs). These were analyzed by XPS before and after thermal treatments and in general were characterized by metallic ratios close to the calculated values. The fifteen catalysts obtained were used in the selective hydrogenation of cinnamaldehyde and the influence of various parameters was studied. The presence of Pt within the clusters greatly improves the selectivity toward COL, as well as bigger particle size that are dependent on the thermal activation: A high activation temperature (1300 °C) was required in this work to reach the best selectivities. The methodology of incorporation also had an impact since a weak bond between metal precursor and carbon surface, such as π - π stacking, will lead to a more significant sintering hence bigger particles, thus influencing positively the selectivity of the reaction. Compared to platinum, gold within clusters shows an opposite tendency and enhances the selectivity toward HCAL. In addition, a modification of solvent in the catalytic reaction changes significantly the selectivity: A same catalyst, for instance **P10-900**, can selectively give COL (51%) in isopropanol/water and HCAL (71%) in toluene. A thermal treatment of graphene beyond 600 °C leads to a high weight loss which limits the activation temperature. Despite this limitation, good results were obtained with this support demonstrating its promising future in this selective hydrogenation reaction. When the best conditions are in place, namely $[\text{Ru}_5\text{PtC}(\text{CO})_{16}]$ as precursor non-covalently immobilized onto MWNTs and thermally treated at 1300 °C, the selectivity toward COL product may reach 75% with good activity (between 70% and 80% conversion for the best catalysts). These catalysts are moreover recyclable without any loss of selectivity and/or activity. Such peculiar synthetic strategy can thus have an attractive future to finely tune the ratio between the different elements by varying the initial ratio between metals within clusters as single source precursors. Moreover, these strategies led to well dispersed particles onto the support and with a narrow size distribution in addition to composition control.

Acknowledgments

We acknowledge the FRS-FNRS, FRIA, Fédération Wallonie-Bruxelles, Loterie Nationale, Belgian State (IAP Project N° P6/17) and Université catholique de Louvain for funding. We are also grateful to Jean-François Statsijns, Cécile Leduff and Michel Genet for technical assistance and fruitful discussions. We also thank Deborah Vidick for some cluster syntheses, Geoffrey Ledent for developments of pyrene strategy and the Nanocyl firm for generous donation of carbon nanotubes.

Appendix A. Supplementary material

Supplementary data associated with this article can be found, in the online version, at <http://dx.doi.org/10.1016/j.jcat.2015.06.003>.

References

- [1] J. Teddy, A. Falqui, A. Corrias, D. Carta, P. Lecante, I. Gerber, P. Serp, *J. Catal.* 278 (2011) 59–70.
- [2] P. Gallezot, D. Richard, *Catal. Rev. Sci. Eng.* 40 (1&2) (1998) 81–126.
- [3] P. Mäki-Arvela, J. Hájek, T. Salmi, D.Y. Murzin, *Appl. Catal. A: Gen.* 292 (2005) 1–49.
- [4] Y. Yuan, S. Yao, M. Wang, S. Lou, N. Yan, *Curr. Org. Chem.* 17 (2013) 400–413.
- [5] U.K. Singh, M. Vannice, *Appl. Catal. A: Gen.* 213 (2001) 1–24.

- [6] H. Ma, L. Wang, L. Chen, C. Dong, W. Yu, T. Huang, Y. Qian, *Catal. Commun.* 8 (2007) 452–456.
- [7] N. Mahata, F. Gonçalves, M.F.R. Pereira, J.L. Figueiredo, *Appl. Catal. A: Gen.* 339 (2008) 159–168.
- [8] G.R. Bertolini, C.I. Cabello, M. Munnoz, M. Casella, D. Gazzoli, I. Pettiti, G.J. Ferraris, *J. Mol. Catal. A: Chem.* 366 (2013) 109–115.
- [9] B.F. Machado, S. Morales-Torres, A.F. Pérez-Cadenas, F.J. Maldonado-Hodar, F. Carrasco-Marin, A.M.T. Silva, J.L. Figueiredo, J.L. Faria, *Appl. Catal. A: Gen.* 425–426 (2012) 161–169.
- [10] A.K. Prashar, S. Mayadevi, R.N. Devi, *Catal. Commun.* 28 (2012) 42–46.
- [11] E. Castillejos, E. Gallegos-Suares, B. Bachiller-Baeza, R. Basca, P. Serp, A. Guerrero-Ruiz, I. Rodriguez-Ramos, *Catal. Commun.* 22 (2012) 79–82.
- [12] A.J. Plomp, D.M.P. van Asten, A.M.J. van der Eerden, P. Mäki-Arvela, D.Y. Murzin, K.P. de Jong, J.H. Bitter, *J. Catal.* 263 (2009) 146–154.
- [13] J. Hajek, N. Kumar, T. Salmi, D.Y. Murzin, *Catal. Today* 100 (2005) 349–353.
- [14] B.M. Reddy, G.M. Kumar, I. Ganesh, A. Khan, *J. Mol. Catal. A: Chem.* 247 (2006) 80–87.
- [15] M. Lashdaf, V.V. Nieminen, M. Tiitta, T. Venäläinen, H. Osterholm, O. Krause, *Microporous Mesoporous Mater.* 75 (2004) 149–158.
- [16] M. Lashdaf, J. Lahtinen, M. Lindblad, T. Venäläinen, A.O.I. Krause, *Appl. Catal. A: Gen.* 276 (2004) 129–137.
- [17] J. Hajek, N. Kumar, P. Mäki-Arvela, T. Salmi, D.Y. Murzin, I. Paseka, T. Heikkilä, E. Laine, P. Laukkanen, J. Väyrynen, *Appl. Catal. A: Gen.* 251 (2003) 385–396.
- [18] J.P. Stassi, P.D. Zgolicz, S.R. de Miguel, O.A. Scelza, *J. Catal.* 306 (2013) 11–29.
- [19] G.R. Bertolini, C.I. Cabello, M. Munnoz, M. Casella, D. Gazzoli, I. Pettiti, G. Ferraris, *J. Mol. Catal. A: Chem.* 366 (2013) 109–115.
- [20] P. Claus, *Top. Catal.* 5 (1998) 51–62.
- [21] N. Job, R. Pirard, J. Marien, J.-P. Pirard, *Carbon* 42 (2004) 619–628.
- [22] Z. Guo, Y. Chen, L. Li, X. Wang, G.L. Haller, Y. Yang, *J. Catal.* 276 (2010) 314–326.
- [23] Y. Li, P.-F. Zhu, R.-X. Zhou, *Appl. Surf. Sci.* 254 (2008) 2609–2614.
- [24] M. Chatterjee, Y. Ikushima, F. Zhao, *New J. Chem.* 27 (2003) 510–513.
- [25] C. Li, Z. Shao, M. Pang, C.T. Williams, X. Zhang, C. Liang, *Ind. Eng. Chem. Res.* 51 (2012) 4934–4941.
- [26] E. Castillejos, M. Jahjah, I. Favier, A. Orejón, C. Pradel, E. Teuma, A.M. Madseu-Bulto, P. Serp, M. Gomez, *ChemCatChem* 4 (2012) 118–122.
- [27] H. Vu, F. Gonçalves, R. Philippe, E. Lamouroux, M. Corrias, Y. Khin, D. Plee, P. Kalck, P. Serp, *J. Catal.* 240 (2006) 18–22.
- [28] M. Sankar, N. Dimitros, P.J. Miedzak, P.P. Wells, C.J. Kiely, G. Hutchings, *J. Chem. Soc. Rev.* 41 (2012) 8099–8139.
- [29] K. Liberikova, R. Touroude, *J. Mol. Catal. A: Chem.* 180 (2002) 221–230.
- [30] S. Recchia, C. Dossi, N. Poli, A. Fusi, L. Sordelli, R. Psaro, *J. Catal.* 184 (1999) 1–4.
- [31] P. Reyes, G. Pecchi, J.L.G. Fierro, *Langmuir* 17 (2000) 522–527.
- [32] P. Reyes, M.C. Aguirre, J.L.G. Fierro, G. Santoni, O. Ferretti, *J. Mol. Catal. A: Chem.* 184 (2002) 431–441.
- [33] P. Reyes, C. Rodrigues, G. Pecchi, J.L.G. Fierro, *Catal. Lett.* 69 (2000) 27–32.
- [34] P. Mäki-Arvela, L.-P. Tiainen, M. Lindblad, K. Demirkan, N. Kumar, R. Sjöholm, T. Ollonqvist, J. Väyrynen, T. Salmi, D.Y. Murzin, *Appl. Catal. A* 241 (2003) 271–288.
- [35] A. Jung, A. Jess, T. Schubert, W. Schütz, *Appl. Catal. A: Gen.* 362 (2009) 95–105.
- [36] F.A. Cotton, *Inorg. Chem.* 3 (1964) 1217–1220.
- [37] J.M. Thomas, B.F.G. Johnson, R. Raja, G. Sankar, P.A. Midgley, *Acc. Chem. Res.* 36 (2003) 20–30.
- [38] R. Raja, T. Khimyak, J.M. Thomas, S. Hermans, B.F.G. Johnson, *Angew. Chem. Int. Ed.* 40 (2001) 4638–4642.
- [39] R. Raja, G. Sankar, S. Hermans, D.S. Shephard, S. Bromley, J.M. Thomas, B.F.G. Johnson, *Chem. Commun.* (1999) 1571–1572.
- [40] M.S. Nasher, D.M. Somerville, P.D. Lane, D.L. Adler, J.R. Shapley, R.G. Nuzzo, *J. Am. Chem. Soc.* 118 (1996) 12964–12974.
- [41] J.M. Thomas, R. Raja, D.W. Lewis, *Angew. Chem. Int. Ed.* 44 (2005) 6456–6482.
- [42] R. Ferrando, J. Jellinek, R.L. Jhonston, *Chem. Rev.* 108 (2008) 845–910.
- [43] J. Shi, R. Nie, P. Chen, Z. Hou, *Catal. Commun.* 41 (2013) 101–105.
- [44] A.J. Plomp, H. Vuori, A.O.I. Krause, K.P. de Jong, J.H. Bitter, *Appl. Catal. A: Gen.* 351 (2008) 9–15.
- [45] M.L. Toebe, Y. Zhang, J. Hájek, T.A. Nijhuis, J.H. Bitter, A.J. van Dillen, D.Y. Murzin, D.C. Koningsberger, K.P. de Jong, *J. Catal.* 226 (2004) 215–225.
- [46] B. Vanhorenbeke, C. Vriamont, F. Penetreau, M. Devillers, O. Riant, S. Hermans, *Chem. Eur. J.* 19 (2013) 852–856.
- [47] C. Janiak, *J. Chem. Soc., Dalton Trans.* (2000) 3885–3896.
- [48] E. Bus, R. Prins, J.A. van Bokhoven, *Catal. Commun.* 8 (2007) 1397–1402.
- [49] C. Milone, C. Crisafulli, R. Ingoglia, L. Schipilliti, S. Galvagno, *Catal. Today* 122 (2007) 341–351.
- [50] H. Rojas, G. Diaz, J.J. Martinez, C. Castaneda, A. Gomez-Cortés, J. Arenas-Alatorre, *J. Mol. Catal. A: Chem.* 363–364 (2012) 122–128.
- [51] J. Lenz, B.C. Campo, M. Alvarez, M.A. Volpe, *J. Catal.* 267 (2009) 50–56.
- [52] X. Zhang, Y.C. Guo, Z.C. Zhang, J.S. Gao, C.M. Xu, *J. Catal.* 292 (2012) 213–226.
- [53] C. Vriamont, M. Devillers, O. Riant, S. Hermans, *Chem. Eur. J.* 19 (2013) 12009–12017.
- [54] S. Hermans, T. Khimyak, N. Feeder, S.J. Teat, B.F.G. Johnson, *Dalton Trans.* (2003) 672–684.
- [55] G. Liu, B. Wu, J. Zhang, X. Wang, M. Shao, J. Wang, *Inorg. Chem.* 48 (2009) 2383–2390.
- [56] F. Li, B. Zhang, X. Li, Y. Jiang, L. Chen, Y. Li, L. Sun, *Angew. Chem.* 123 (2011) 12484–12487.
- [57] L. Xing, J.-H. Xie, Y.-S. Chen, L.-X. Wang, Q.-L. Zhou, *Adv. Synth. Catal.* 350 (2008) 1013–1016.
- [58] P.D. Tran, A. Le Goff, J. Heidkamp, B. Jousseme, N. Guillet, S. Palacin, H. Dau, M. Fontecave, V. Artero, *Angew. Chem. Int. Ed.* 50 (2011) 1371–1374.
- [59] S. Hermans, T. Khimyak, B.F.G. Johnson, *J. Chem. Soc., Dalton Trans.* (2001) 3295–3302.
- [60] T. Khimyak, B.F.G. Johnson, S. Hermans, A.D. Bond, *Dalton Trans.* (2003) 2651–2657.
- [61] M.I. Bruce, E. Horn, P.A. Humphrey, E.R.T. Tiekink, *J. Organomet. Chem.* 518 (1996) 121–138.
- [62] G.W. Smith, E.A. Carter, *J. Phys. Chem.* 95 (1991) 2327–2339.
- [63] J.A. Martinho Simoes, J.L. Beauchamp, *Chem. Rev.* 90 (1990) 629–688.
- [64] S. Hermans, V. Bruyr, M. Devillers, *J. Mater. Chem.* 22 (2012) 14479–14486.
- [65] D. Vidick, M. Herlitschke, C. Poleunis, A. Delcorte, R.P. Hermann, M. Devillers, S. Hermans, *J. Mater. Chem. A* 1 (2013) 2050–2063.
- [66] C. Willocq, D. Vidick, B. Tinant, A. Delcorte, P. Bertrand, M. Devillers, S. Hermans, *Eur. J. Inorg. Chem.* (2011) 4721–4729.
- [67] E. Castillejos, P.J. Debouttiere, L. Roiban, A. Solhy, V. Martinez, Y. Kihn, O. Ersen, K. Philippot, B. Chaudret, P. Serp, *Angew. Chem.* 48 (2009) 2529–2533.